An investigation of branch stresses induced by arboricultural operations

Ignacio Cetrangolo[a], Sanjay R. Arwade[a,*], Brian Kane[b]

[a] *Department of Civil & Environmental Engineering, University of Massachusetts, Amherst, 01003, USA*
[b] *Department of Environmental Conservation, University of Massachusetts, Amherst, 01003, USA*

ARTICLE INFO

ABSTRACT

This paper presents a method for assessing the safety of tree branches subject to unorthodox climbing approaches and possible falls. The method entails finite element modeling of the tree branch, experimentally or analytically determining loads associated with an ascending or falling climber, and computing stresses and safety factor along the length of the branch using dynamic structural analysis. A case study example is presented for an *Ulmus americana* L. branch on the campus of the University of Massachusetts, Amherst. This tree and branch were climbed using an unorthodox and controversial method during a competition in 2014. Case study models demonstrate that during an ascent, a climber's skill has a significant effect on branch stresses, and during a simulated fall, the climber's mass and fall distance are the key determinants of branch stresses. For loads induced during an ascent, safety factors for branches ranged between 3 and 4; for loads induced during a fall, safety factors were as low as 1.2. These values are dangerously low given the uncertainty of branch material properties. Climbers should be extremely cautious when attempting unorthodox climbing techniques.

1. Introduction

Arboriculture is a dangerous profession in which 14.1 fatalities per 100,000 workers involved in tree work [1] were reported in 2003, much greater than the overall population rate of 4.0 fatalities per 100,000 workers (Wiatrowski, 2005). Of the 1285 arboriculture worker fatalities between 1992 and 2007, 44% occurred while pruning or trimming trees, and 34% involved a fall (Castillo and Menéndez, 2009). The Center for Disease Control's National Institute for Occupational Safety and Health (NIOSH) explicitly recommends, "checking the condition of tree branches before…climbing," (Castillo and Menéndez, 2009), but: (1) climbers cannot carefully inspect a branch until they are close to it, (2) climbers cannot assess internal structural defects or ascertain the severity of external structural defects without sophisticated measuring devices and (3) there is a lack of robust data quantifying the safety of branches under expected or "worst-case-scenario" loads.

This paper introduces a method for assessing the safety of a branch when loaded by an ascending or falling climber, and shows how the stresses depend on the type of ascent and parameters of the fall. Following description of the method, results are presented for an example branch subject to a variety of ascending and falling loads. The findings point to ways in which arborist safety can be enhanced even in the absence of engineering analysis of the tree branch.

The work presented here is motivated by observations of an unorthodox and potentially dangerous ascending technique during a

competition in 2014 in Massachusetts. To encourage worker safety, safe work practices are strongly emphasized at contemporary climbing competitions (http://www.itcc-isa.com/about/missionhistory/history. aspx, http://www.itcc-isa.com/resources/about_Eventdescriptions_ MastersChallenge.pdf). During a Masters' Challenge event in 2014 in Massachusetts, a competitor installed the rope over a distal portion of a branch and footlocked the doubled rope (Adams, 2007) to reach one of the work stations in the event rather than ascending to the top of the tree and limb-walking in the conventional fashion (with the anchor point over a branch and around the main stem (Fig. 1) at a central point near the top of the crown (Lilly, 2005). Conventional limb-walking facilitates lateral movement throughout the crown with continuous rope support from a point higher in the crown. Limb-walking provides maximum stability for a climber and minimizes the bending moment on the branch (because the rope carries part of the climber's weight).

Prior to the competitor's ascent, judges conferred about the safety of the unorthodox approach and allowed the competitor to continue since the branch was large and *Ulmus americana* L. is considered to have strong wood. The branch supported the applied loads during ascent and descent without failure or apparent damage. Thankfully, the climber did not fall, but loads induced by a falling climber would be much greater, and the event inspired this study. The objective of this paper is to define a method for assessing branch safety using the case study of the *U. americana* branch. The results of the analyses provide guidance to climbers about branch safety during ascent or a fall.

---

* Corresponding author at: 223 Marston Hall, CEE, University of Massachusetts, Amherst, 01003, USA.
E-mail address: arwade@umass.edu (S.R. Arwade).

Fig. 1. Proper tie-in for work-positioning: a climber's rope passes over a lateral branch (on the right) and around the main stem.

2. Methods

The method used to address the objective of this paper consists of four steps: (i) definition of general branch geometry and section properties, and the internal forces, stresses and safety factors in general terms; (ii) description of the branch analyzed in this paper, including wood properties; (iii) determination of ascending and falling loads by experimental or analytical methods; (iv) development of a finite element model for the purposes of static, modal, and dynamic time history analysis. This method applies generally to the analysis of tree branches subjected to loads that could occur during an ascent or a fall, and is useful because it provides a framework for continued research into climber safety. The following sub-sections describe the four steps.

2.1. General definitions

Throughout the text, the branch described in the introduction is referred to as the primary branch—a branch that arises from the main stem or trunk. Lateral branches arising from the primary branch are referred to as secondary branches. The geometry of a primary branch can be defined by the parameterized coordinates $(x(s_1), y(s_1), z(s_1))$, where s_1 is a local, curvilinear coordinate that has its origin at the attachment of the branch to the trunk. The coordinate system is defined such that z is positive upward and the x and y coordinates define a plane parallel to the ground. The local coordinate specifies, for $0 < s_1 < l_1$, position along the length of the main branch, which has a total length l_1. The geometry of secondary branches is described by $(x(s_{2,i}), y(s_{2,i}), z(s_{2,i}))$, where $0 < s_{2,i} < l_{2,i}$ is the local curvilinear coordinate for the ith secondary branch that is of length $l_{2,i}$ and has its origin at the attachment point to the primary branch $s_{1,i}$.

Ignoring shear deformations, the spatially varying moment of inertia $I(s)$, torsional constant $J(s)$ and cross-sectional area $A(s)$ are the complete set of section properties for a circular branch, and depend on the branch diameter $d(s)$. Tree branches are not generally circular, with the depth often exceeding the width. Circularity of the cross section is assumed here, though the approach could be readily adapted to treat branches with elliptical or other cross sections. Details about the validity of this assumption for the example tree are given in Section 2.2.

In this paper, only the response of the primary branch is considered, and the key response quantities are the: (i) displacements $(u(s_1,t), v(s_1,t), w(s_1,t))$ corresponding to the (x, y, z) coordinate directions where z is the downward direction and the x and y directions are in the plane parallel to the ground, (ii) bending moments $(M_p(s_1,t), M_q(s_1,t))$ which correspond to vertical and lateral bending of the branch, and (iii) axial force $N(s_1,t)$. The two bending moments act with respect to orthogonal,

cross-sectional coordinates (p, q) and can be combined into a resultant bending moment $M_r(s_1, t) = \sqrt{M_p(s_1, t)^2 + M_q(s_1, t)^2}$. The axial force and resultant bending moment generate stresses that can be combined to yield a maximum compressive stress, which acts along the longitudinal axis of the branch and occurs in the outer wood fibers at the bottom of the branch cross-section:

$$\sigma_{c,max}(s_1, t) = \left| \frac{M_r(s_1, t)d(s_1)}{2I(s_1)} \right| + \left| \frac{N(s_1, t)}{A(s_1)} \right| \tag{1}$$

The maximum stress that occurs at any point along the branch and at any time of the analysis is $\sigma_{c,max} = max_{(s_1,t)}(\sigma_{c,max}(s_1, t))$ and the location at which that maximum stress occurs is $s_{1,max} = \text{argmax}_{s_1}((\sigma_{c,max}(s_1, t)))$. Safety is checked by evaluating the safety factor $FS = \sigma_{c,all}/\sigma_{c,max}$. If $FS \geq 1$ the limb is safe, if $FS < 1$ the branch is unsafe and is predicted to fail under the current set of assumptions. Shear and torsional stresses were neglected in this analysis because the primary branch is slender (span:depth ratio > 30) and torsional loads are minimal since the branch was relatively straight between the trunk and the load point.

2.2. An example tree and branch

The *U. americana* tree that inspired this study is shown in Fig. 2. The branch was measured at increments of $\Delta s_1 = 1$ m out to $s_1 = 11$ m, and a final measurement was taken at $s_1 = 11.5$ m, which is the point of load application (s_{load}) and the point at which the primary branch divided into two secondary branches. At each increment, the depth and width, azimuth and elevation angle of the primary branch were recorded. Subsequently, the azimuth and elevation angle were converted to Cartesian coordinates $(x(k\Delta s_1), y(k\Delta s_1), z(k\Delta s_1))$, $k = 1, 2, …, 11, 11.5$ with $\Delta s_1 = 1$m (Table 1). The cross section is approximated as circular and the diameter reported in Table 1 is the average of the measured width and depth. This assumption simplifies the analysis and, for the example tree, results in an error in cross section moment of inertia of no more than 7% (in only 1 segment). In 3 of the measured segments the cross section width and depth were equal.

Three secondary branches were present, including extension of the primary branch past the final measurement point. Secondary branch measurements were limited to (i) the location of their attachment point $(s_{1,1}, s_{1,2}, s_{1,3})$, (ii) the diameter at that point, and (iii) the distance to the distal end of the secondary branch (Table 2). This distance is used to approximate the secondary branch lengths $(l_{2,1}, l_{2,2}, l_{2,3})$. Since cross-sectional measurements of the secondary branches could not be practically obtained, the secondary branches were approximated as cones with diameter that tapered linearly from the proximal to the distal end so that the diameter of each secondary branch is given by $d(s_{2,i}) = d(s_{2,i} = 0)((l_{2,i} - s_{2,i})/l_{2,i})$. While this conical form does not exactly represent secondary branch geometry it is adopted as a simple approach to including secondary branch mass distribution in dynamic analysis.

Branch diameters shown in Tables 1 and 2 were measured outside of the bark. To avoid unnecessary wounding, bark thickness was measured at four points along the branch (rather than every meter). From these measurements, the bark thickness t_b is assumed to be

$$t_b(s_1) = \begin{cases} 1.25 \text{ cm} & s_1 < 3 \text{ m} \\ 0.60 \text{ cm} & 3 \text{ m} < s_1 < 6 \text{ m} \\ 0.40 \text{ cm} & 6 \text{ m} < s_1 < 9 \text{ m} \\ 0.20 \text{ cm} & 9 \text{ m} < s_1 < 11.5 \text{ m} \end{cases} \tag{2}$$

Assuming that bark does not contribute to structural stiffness, the moment of inertia is $I(s_1) = \pi(d(s_1) - t_b(s_1))^4/32$, the cross-sectional area is $A(s_1) = \frac{\pi(d(s_1) - t_b(s_1))^2}{4}$, and the torsional constant is $J(s_1) = \pi(d(s_1) - t_b(s_1))^4/16$. Bark thickness was assumed constant at 0.20 cm for secondary branches.

The compressive bending strength of branch wood parallel to grain, $\sigma_{c,all}$, was assumed to be 75% of the MOR reported in Kretschmann (2010) for green *U. americana*. The reported value of MOR is 50 MPa
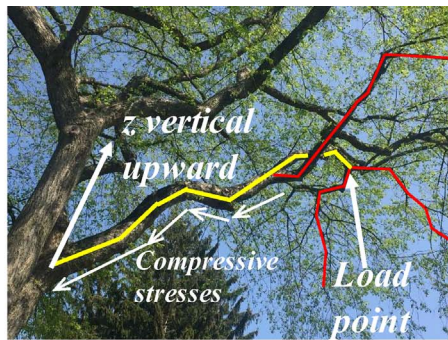
Fig. 2. *Ulmus americana* L. located on the campus of the University of Massachusetts, Amherst, including (a) an image from September 2016 (z direction is positive upward), and SketchUp models from (b) the same perspective as the image and (c) above (in the −z direction). The (x,y) plane is parallel to the ground, and primary and secondary branches are indicated by yellow and red lines, respectively. The load point is also indicated.. (For interpretation of the references to colour in this figure legend, the reader is referred to the web version of this article.)

(a) Image of branch (primary branch in yellow, secondary branches in red), showing load application point, z coordinate direction, and location of compressive stresses. Compressive stresses are longitudinal and occur along the bottom surface of the branch
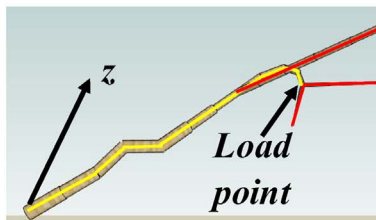
(b) SketchUp model of branch from same perspective as (a)
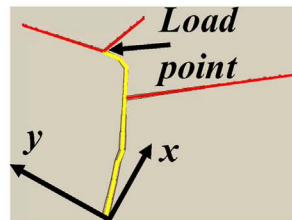
(c) SketchUp model of branch showing x and y coordinate directions in a plane parallel to the ground

and the reduced value is therefore $\sigma_{c,all}$ = 37.5 MPa. The reduction was applied because previous studies have demonstrated that the breaking strength of trunks (Kane, 2014; Kane and Clouston, 2008) or branches (Kane, 2007) is 20% to 40% less than the MOR of small, defect free, specimens taken from the trunk or branch, and Okai et al. (2004) have also reported different strengths for branch wood when compared to trunk wood.

2.3. Applied loads

Four types of loading (all in the downward or −z direction) are considered in this paper: (i) static self-weight of the branch, (ii) a static point load that represents the static weight of a climber, (iii) a dynamic time history point load that represents load applied to the branch during an ascent, and (iv) a dynamic time history point load that represents load applied to the branch during the arrest of a fall. When loading involved a climber (types ii, iii, iv), the application point of the

Table 2
Secondary branch geometry.

Secondary branch number	Attachment point − $s_{1,i}$ (m)	Diameter at attachment − $d(s_{2,i} = 0)$ (cm)	Length l_{2i} (m)
1	11.5	15.4	7.3
2	11.5	12	6
3	7	21.6	11

load was s_{load} = 11.5 m.

Self-weight of the *U. americana* branch (N/m) is the product of gravitational acceleration with the cross-sectional area and mass density of the branch wood, assumed to be 1050 kg/m³ (Glass and Zelinka, 2010). Branch cross-sectional area was calculated excluding bark.

The static point load was used to calibrate the structural elastic modulus $E*$ (Brüchert et al., 2003), which was used in the finite element model (sub-section 2.4). The structural elastic modulus captures the

Table 1
Primary branch geometry and associated Cartesian coordinates $(x(s_1), y(s_1), z(s_1))$. Azimuth and elevation angle were measured at the distal point of each branch segment so no azimuth or elevation angle was recorded for measurement location $s_1 = 0$.

Measurement location − s_1 (m)	Diameter $d(s_1)$ (cm)	Azimuth (deg)	Elevation angle (deg)	$x(s_1)$ (m)	$y(s_1)$ (m)	$z(s_1)$ (m)
0	38	N/A	N/A	0	0	0
1	38	68	58	0.78	0.31	0.52
2	35	68	58	1.57	0.63	1.05
3	33.9	68	44	2.21	0.89	1.77
4	33.9	66	88	3.12	1.30	1.81
5	35.8	55	53	3.78	1.76	2.41
6	29	55	53	4.43	2.21	3.01
7	21	55	53	5.09	2.67	3.61
8	19.9	55	53	5.74	3.13	4.22
9	21.2	55	65	6.48	3.65	4.64
10	20	26	82	6.92	4.54	4.78
11	15.5	6	90	7.02	5.53	4.78
11.5	15.4	6	90	7.07	6.03	4.78

overall stiffness of the branch rather than representing the elastic modulus of the wood itself, which varies spatially within the cross section and along the length of the branch. Structural elastic modulus is used since it was not possible to sample wood directly from the branch and wood properties can vary radially and axially (Niklas, 1997). To determine E^*, a climber (mass = 77 kg, weight = 755 N) suspended himself from the branch at load location s_{load} and a branch deflection of 7.6 cm was measured at s_{load}. Subsequently, E^* of the branch was adjusted in the finite element model until the modeled branch deflection at s_{load} was 7.6 cm: $E^* = 11,900$ MPa. This value is applied uniformly throughout the branch model.

2.3.1. Loads during an ascent

To model the load experienced by the *U. americana* branch during an ascent, experimental data from two male climbers (climber 1 and climber 2) was used. Neither of these climbers was the same individual as used in the static test to determine the structural elastic modulus. Including gear, each climber weighed 883 N (90 kg), and each ascended on Sterling Super Static rope (11 mm diameter, 29,000 N minimum breaking strength (MBS), and 8.5% elasticity—defined as percent strain at 10% of MBS; https://sterlingrope.com/store/work/ropes/static/superstatic2/7-16-superstatic2). The rope was arranged in a stationary rope system (SRS) (http://www.itcc-isa.com/resources/rules_ITCC_v2016.pdf), and each climber ascended using two techniques: footlocking a doubled rope and using hand and foot ascenders to ascend a single rope anchored at the base of the tree ("single rope technique"). Each climber performed each technique twice, while rope tensions accurate to 10 N were recorded at 10 Hz using Dillon EdXtreme dynamometers (Weigh-Tronix, Fairmont, MN), yielding eight load time histories of an ascent.

Load time histories of climbers 1 and 2 were denoted by a three character code specifying the technique (F = footlocking, S = single rope), the climber (1, 2) and the trial (1, 2). For example, F-2-1 indicates the first trial of the second climber using footlocking technique.

2.3.2. Loads during a fall

It was not safe to measure loads during a climber's fall experimentally; instead, they were calculated based on principles of dynamics. A hypothetical climber was assumed to be in the process of ascending a single or doubled rope in a SRS when a fall occurred. The arrest of the fall caused a dynamic load on the branch. Loads induced during a fall are defined by (i) the mass of the climber m, (ii) the length of rope between the climber and the branch at the time the fall is arrested l_r, (iii) the fall distance l_f, and (iv) the elasticity of the rope ε_{10mbs}. The range of values used for each of the four parameters is in Table 3. Note that the climber described in this section is hypothetical, since physical experiments were deemed unsafe, and therefore suitable ranges of parameters could be chosen that do not necessarily correspond to the actual climbers used in determination of ascending loads. Of particular note, the climber masses of 81.6 kg (180 lbs) and 99.8 kg (200lbs) were chosen to be broadly reflective of a range of climber-plus-gear weights encountered in the profession. The calculation of load time histories of a falling climber was based on a single degree of freedom system in which the climber is the mass, the rope is the spring, and the *U. americana* branch provides the boundary condition supporting the spring. The branch is flexible, with stiffness k_b (measured at 9900 N/m),

Table 3
The range of values in each parameter needed for the theoretical calculation of the load induced during a climber's fall.

Climber mass, m (kg)	Fall distance, l_f (m)	Rope length, l_r (m)	Rope elasticity, ε_{10mbs} (%)
81.6, 99.8	0.99, 1.32	1.52, 3.05, 6.10, 9.14, 12.14	1, 2, 3, 4, 5

and the stiffness of the rope is:

$$k_r = \left(\frac{0.1 f_{mbs}}{\varepsilon_{10mbs} l_r} \right) \tag{3}$$

where f_{mbs} is the minimum breaking strength of the rope, taken as 29,813 N. The total stiffness of the system is $k = (1/k_b + 1/k_r)^{-1}$. The position of the climber during the fall is given by the coordinate $z_c = -(z + l_r + mg/k)$, defined so that $z_c = 0$ is the static equilibrium position of the climber hanging on the rope and $z_c > 0$ represents displacement toward the ground. During the fall, the force in the rope is $f(t) = k z_c(t) + mg$ and the solution of the governing equation for $z_c(t)$ is

$$z_c(t) = z_c(0)\cos(\omega_n t) + \frac{\dot{z}_c(0)}{\omega_n}\sin(\omega_n t) \tag{4}$$

with initial conditions $z_c(0) = -mg/k$ and $\dot{z}_c(0) = \sqrt{2gl_f}$ and natural frequency $\omega_n = (k/m)^{1/2}$. Gravitational acceleration is g.

If the climber-branch-rope system is elastic and undamped, the climber will rebound to a position higher than the point at which the fall begins to be arrested ($x(t) < -mg/k$). At that point, the force in the rope becomes zero until the line becomes taut again. The time at which the rope force becomes zero due to this rebound is $t_f = \text{argmin}_t\ (x(t) < -mg/k)$, the minimum value of t at which the rope becomes slack, and the load history applied to the branch is

$$f(t) = \begin{cases} k z_c(t) + mg & 0 \le t \le t_f \\ 0 & t_f < t \end{cases} \tag{5}$$

Load time histories were calculated for every combination of parameters in Table 3: 100 load time histories in total. Each load time history was identified by a 4-number code where the numbers, in order, denote the climber mass (kg), fall distance (m), rope length (m), and rope elasticity (%) (from Table 3). For example, 81.6-1.32-1.52-3 denotes a case with a climber mass of 81.6 kg, a fall distance of 1.32 m, a rope length of 1.52 m, and a rope elasticity of 3%.

2.4. Finite element modeling and analysis

A finite element model of the *U. americana* branch was developed to calibrate the structural elastic modulus (E^*) of the branch wood and to model the dynamic response of the branch to loads induced during an ascent or fall. The finite element method is the primary tool used by engineers to simulate the performance of structural and mechanical systems under load.

This section describes idealizations and assumptions used to construct a finite element model of the *U. americana* branch. Attachment of the primary branch to the trunk was assumed to be fully fixed, its cross section is assumed circular, and bark contributions to cross-sectional properties were neglected.

The finite element model was constructed in the commercial analysis package ADINA (Bathe 2006, Fig. 3) using three-dimensional Euler-Bernoulli beam elements with constant cross section. Matching the element length to the distance between measurement points (1 m in all cases except the two measurement points at $s_1 = 11$ m, 11.5 m) provided converged results. Therefore, node locations correspond to measurement points in Table 1 for the primary branch and were spaced in increments of $\Delta s_{2,i} = 1$m for the secondary branches. Section properties for each finite element were computed based on the average of the diameter at each end of the element.

Three types of analysis were performed on the finite element model: static analysis, modal analysis, and dynamic time history analysis. Details on the mathematics of these analyses can be found, for example, in Bathe (2006), and summaries of the key features of each analysis type are provided here. Static analysis provides displacements and internal forces (moments, shears, and axial force) at each node of the model for without consideration of dynamic effects. This analysis type was used to calibrate E^* of the branch wood. Modal analysis provides
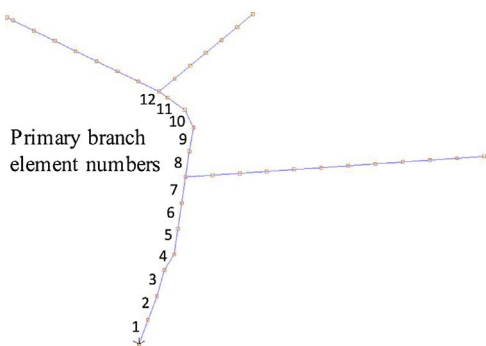
Fig. 3. Finite element model of *Ulmus americana* L. branch shown in Fig. 2, including twelve elements used to mesh the primary branch. Load application is at the distal node of element 12, where the primary branch divided into two secondary branches. Nodes are shown on secondary branches.

the frequencies or periods at which the modeled *U. americana* branch naturally vibrates, and their corresponding mode shapes. Modal analysis is independent of the loading and the results depend only on the geometry, boundary conditions, and material properties of the branch. Modal analysis was used to aid in understanding of branch behavior and to provide insight into the role of load duration in generating branch response. Dynamic time history analysis directly integrates the dynamic equation of branch motion and provides nodal displacements and internal forces at each time step of the simulation. Dynamic time history analysis was used here to model the response of the branch to measured (sub-section 2.3.2) and calculated (sub-section 2.3.1) loads induced during an ascent and fall, respectively. In the dynamic time history analyses, damping of 5% was assumed, and a time step of 0.005 s provided converged results.

3. Results and discussion

3.1. Loads induced during an ascent

The load time histories of all eight trials (Fig. 4) show a rapid increase in load as the climber begins his ascent followed by a period of cyclic loading as the climber incrementally hauls himself up the rope, and then a rapid decrease in loading as the branch is reached and the rope is unloaded. The mean load during the footlocking ascent is approximately equal to the climber's weight and the mean load during the single rope ascent is related to the climber's weight, the angle of the anchor end of the rope, and frictional losses at the rope-branch interface. There was significant variation in the characteristics of the loading histories due to each climber's proficiency with each ascent technique. For example, although mean loads were similar in the footlocking trials for climber 1 and climber 2, climber 1 caused significantly larger cyclic amplitudes while ascending. The duration of load also varies, particularly when ascending a single rope, when climber 1 took significantly longer to ascend. In one of the footlocking trials, data logging failed before completion of the ascent.

3.2. Loads induced during a fall

Fig. 5 shows the 100 load time histories corresponding to every combination of the parameters in Table 3. Only loads for a fall induced during a single rope ascent are shown; the effects of falling while footlocking a doubled rope are included in the Discussion. The load time histories cover a realistic range of fall distances, rope lengths, climber masses, and rope elasticities, and have a range of peak loads and durations. The maximum peak load of 6000 N reflects a dynamic amplification of 6 times with respect to the static load for the equivalent climber. Fig. 5 is annotated with text and lines to show the branch vertical mode half period and the cases that lead to the maximum force and maximum and minimum branch stresses (sub-section 3.4).
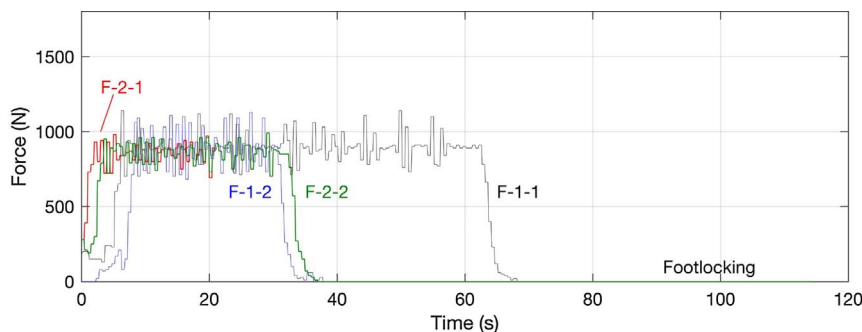
(a) Four load time histories for footlocking ascents **of two different climbers each repeating the ascent two times**.
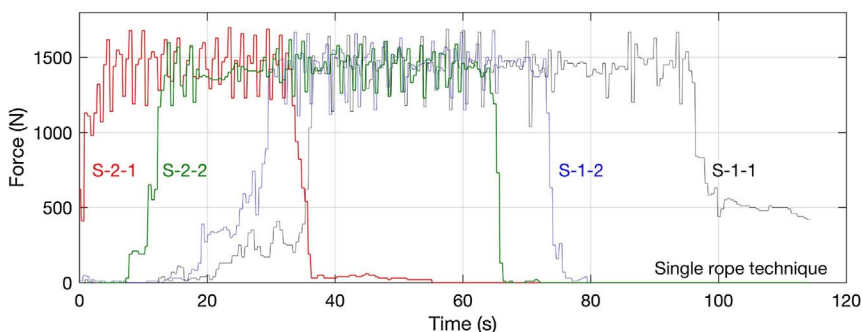
(b) Load time histories for single rope technique ascents of two different climbers each repeating the ascent two times.

Fig. 4. Load time histories for ascent on a stationary rope system. Two climbers performed two trials each (a) by footlocking a doubled rope and (b) on a single rope using ascenders. Each time history is labeled by three-character code representing, in order, the ascent method (F = footlocking, S = single rope), climber (1, 2) and trial (1, 2).
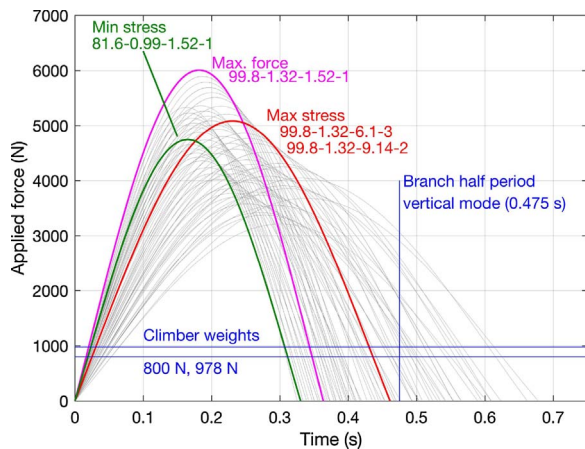
Fig. 5. Load time histories (light grey) calculated for every combination of parameters listed in Table 3. Load time histories have a significant range of durations and amplitudes. Amplitudes are well in excess of the assumed static weight of the climbers and durations span across the first vertical mode period of the branch. Annotations indicate the fall parameters (numbers separated by dashes that correspond to values in Table 3) that lead to the largest force and the maximum and minimum branch stresses.

3.3. Modal analysis

Modal analysis of the *U. americana* branch model provided the first vertical bending mode shape shown in Fig. 6. The corresponding frequency of the first vertical bending mode was 0.95 Hz (1.06 s period). The frequency was comparable to the cycle frequency of loads induced during an ascent (Fig. 4), and the natural period was roughly twice the duration of the load pulse in the falling case (Fig. 5).

3.4. Dynamic time history analysis

Dynamic time history analysis of the loads measured during an ascent or calculated during a fall on a single rope yielded two responses in each element in the modeled *U. americana* branch: vertical displacement and $\sigma_{c,max}(t)$. Examples of displacement time histories generated by the finite element model from load time histories of a measured ascent (F-1-1) and a calculated fall (81.6-0.99-1.52-1) are shown in Fig. 7. The displacement time histories show the vertical branch displacement at s_{load}. For F-1-1, oscillations in the displacement closely matched the cycles in the applied load, and the response to 81.6-0.99-1.52-1 corresponded to that of a simple harmonic oscillator forced by an impulse load. In Fig. 7, branch response to the load induced by a fall after $t = 0.65$ s was neglected in the analysis since it corresponds to the time when the climber has rebounded upward from the initial fall arrest. Time histories of $\sigma_{c,max}(t)$, closely follow those in Fig. 7.

Table 4 shows $\sigma_{c,max}$ that occurred during the measured ascent trials shown in Fig. 4. Loads measured during single rope technique ascents induced $\sigma_{c,max}$, that is, on average, 37% greater than footlocking. Climber proficiency also had a strong effect on $\sigma_{c,max}$, with climber 1 inducing greater stress than climber 2. The difference between climbers
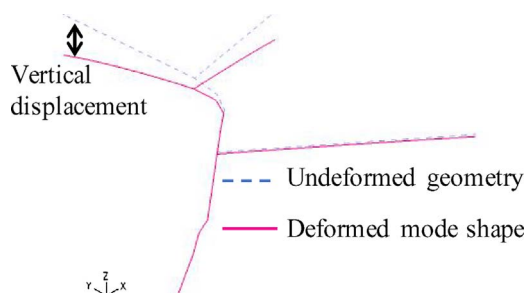

Fig. 6. First vertical bending mode shape of the tree branch at 0.95 Hz (Period = 1.05 s).

is 6.5% for single rope ascent and 19% for footlocking. Since the climbers' masses were within 1 kg of each other, differences in $\sigma_{c,max}$ reflect differences in proficiency. Climber 1 had much less experience footlocking, and struggled to ascend smoothly. Lack of smoothness during ascent induced greater loads, evident in Fig. 4. Training to improve a climber's proficiency may meaningfully reduce the stress during ascending, enhancing worker safety.

For values of $\sigma_{c,max}$ during ascent, $FS = 3$ for single rope and $FS = 4$ for footlocking. On a decayed branch, FS would be less because decay reduces the moment of inertia $I(s_1)$ (Kane and Ryan, 2004). Other defects (e.g., cracks, weak attachments) also reduce FS, and may not be visible during a pre-climb inspection from the ground. If the defects occur on the upper surface of an anchor point, even using binoculars might not reveal the defects. Given that FS for engineered civil structures are often close to 2 (Salmon and Johnson, 1990) $3 < FS < 4$ should not be considered excessive. For comparison, FS for the components of a climbing system are 13 (Anonymous, 2013).

Fig. 8 shows $\sigma_{c,max}$ for all of the falling load cases, organized by fall parameter values: climber mass, fall length, rope length, and rope elasticity. The range of maximum stresses is significant, with a minimum value of 23.6 MPa giving $FS = 1.6$ (case 81.65-0.99-1.52-1) and a maximum value of 32.4 MPa giving FS = 1.2 (cases 99.8-1.32-6.1-3 and 99.8-1.32-9.14-2). The safety factors are dangerously small given model and analysis uncertainties, and the range of stresses represents 24% of the allowable stress of 37.5 MPa, meaning that differences in climber mass and fall distance and other parameters over ranges that could be expected to occur in practice may be sufficient to determine whether a branch fails during fall arrest. There were 16 falling load cases that produce maximum stresses within 1% of the maximum value of 32.4 MPa, all involving the heavier climber falling the longer distance. The values of rope length and rope elasticity that result in maximum and minimum stress are not at the extremes, and each value of those parameters is represented in the group of 18 cases that produce stresses within 1% of the maximum. Neither the longest most compliant rope, nor the shortest, stiffest rope consistently corresponded to maximum or minimum stress in the branch during a fall. Rope properties cannot be directly connected to branch stresses because of the dynamic character of the problem. Dynamic response and stresses are maximized when the loading duration coincides with half of the first vertical mode period of the branch. Therefore, a rope that is very stiff will result in a loading duration that is too short to generate maximum stress and a rope that is very flexible will result in a loading duration that is too long to generate maximum stress. For this branch, coincidence of the loading duration and branch half period occurred for intermediate values of rope stiffness.

The interplay between loading parameters and response parameters is also shown graphically in Fig. 4, which shows that the fall that induced the maximum force on the branch did not induce maximum stress in the branch because the load duration was significantly shorter than the branch half period. Minimum branch stress was induced by the fall that resulted in the shortest duration load (this case also had a low amplitude of maximum force), and the maximum branch stress was induced by falls that generated loads with durations very close to the branch half period. Branch stresses were highly sensitive to the overall dynamics of the climber-rope-branch system, with coincidence between the load duration and the branch half period being a key determiner of response magnitude.

Though climber mass and fall length both significantly controlled stresses, mass was the most important factor. Mass and fall length define the energy of the fall that must be arrested by the rope, and the rope length and rope elasticity define the stiffness of the rope k_r. The mass contributed to branch response by increasing, linearly, the amplitude of the dynamic oscillation ($x(0) \propto m$) and by increasing the static force mg. The fall length (l_f), on the other hand, appears only to the ½ power in $\dot{x}(0) = \sqrt{2gl_f}$, meaning that branch response is more sensitive to climber mass than fall length, although fall length is still
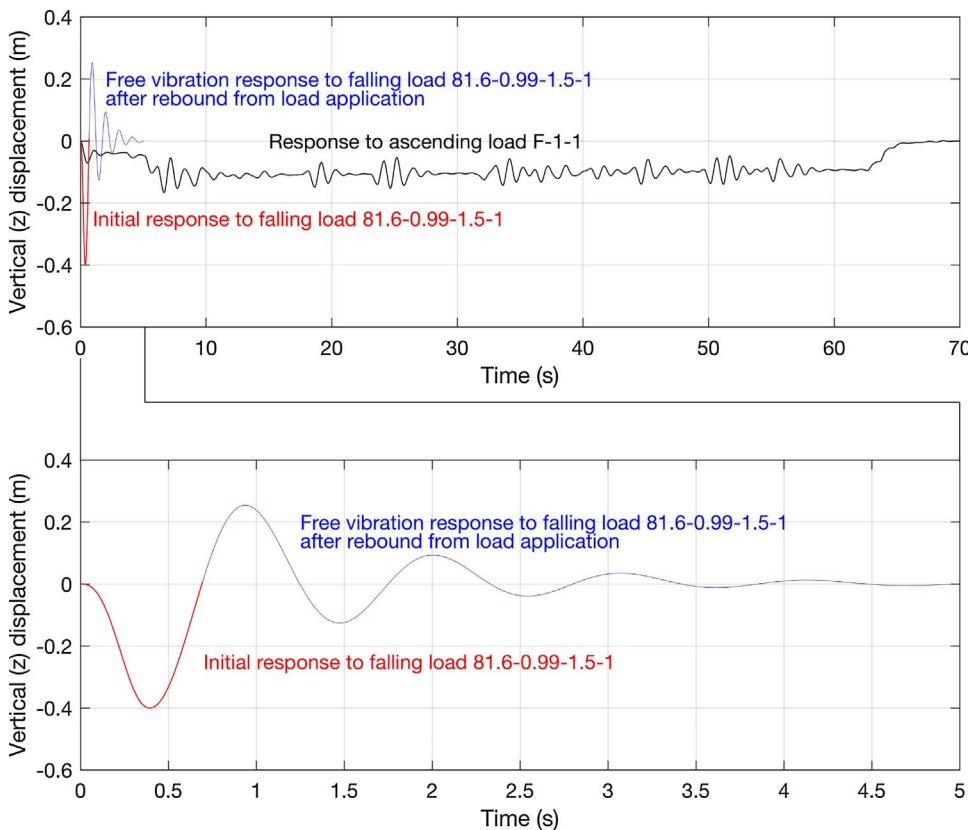
Fig. 7. Examples of *Ulmus americana* L. branch displacement time histories at the load application point s_{load} = 11.5 m for loads measured during an ascent (the first trial of climber 1 footlocking a doubled rope (F-1-1)) and calculated for a fall on a single rope anchored in the crow (assuming a climber of mass 81.6 kg who falls 0.99 m with 1.5 m of rope with 1% elasticity in the system (81.6-0.99-1.5-1)). The top frame shows the complete time history of displacements for both cases. The bottom frame shows case 81.6-0.99-1.5-1 in detail. Since the bouncing of the falling climber on the rope is not simulated in the load time histories, the part of the response to a load induced during a fall after the displacement up-crosses 0 m (t = 0.65 s) was neglected.

Table 4

Maximum stresses (MPa) induced during eight ascents: two trials of two climbers using two techniques. In each trial, maximum stress occurred in element 7 (Fig. 3) of the finite element model. Shaded cells contain the maximum stress values from each ascent trial. Unshaded cells contain averages for each climber using each technique and of each technique for both climbers.

Ascent technique	Climber 1	Climber 2	Average by technique
Single Rope	12.7, 12.7	12.1, 11.8	12.3
Average of two trials	12.7	11.9	
Footlocking	9.5, 9.9	8.4, 7.8	8.9
Average of two trials	9.7	8.2	
Average by climber	11.2	10.1	

more important than rope length or elasticity.

Even though the response was primarily governed by m and l_f, k_r (as defined by l_r and ε_{10mbs}) did play a role in determining the stress in the branch. In Fig. 8, within each ml_f group, the maximum stress varied by as much as 1.25 MPa over the range of l_r and ε_{10mbs} considered in this study, 3% of the allowable stress.

Stresses for a fall during footlocking can be obtained from those for a fall during a single rope technique ascent with an effective rope elasticity of $2\varepsilon_{10mbs}$ since footlocking involves a doubled rope.

The range in maximum branch stresses induced during a fall corresponded to a range in *FS* from 1.6 (case 81.65-0.99-1.52-1) to 1.2 (cases 99.8-1.32-6.1-3 and 99.8-1.32-9.14-2), which are dangerously small.
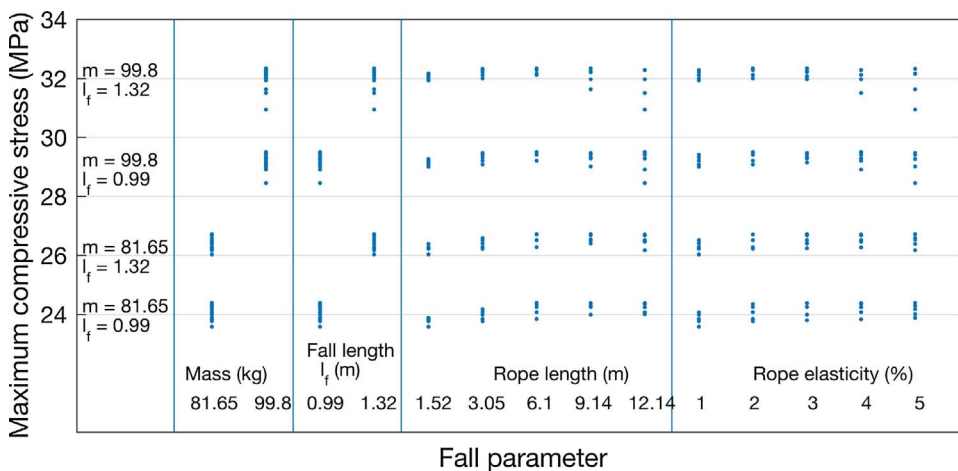

Fig. 8. Influence of fall parameters on maximum combined stress in the branch ($\sigma_{c,max}$) in MPa, which always occurred in segment 7, regardless of the combination of parameters. Parameter values are shown in groups along the horizontal axis. Four horizontal bands of data correspond to pairs of mass and fall length (m, l_f) as shown along the left vertical axis.

3.5. Further discussion

In the finite element model, $\sigma_{c,max}$ occured in element 7 (6 m $< s_1 <$ 7 m) for all loads induced during an ascent or fall. Bending moment and branch diameter increased toward the proximal end of the branch (i.e., decreasing s_1), but the increase in bending moment is linear, while $I \propto d^4$, $c \propto d$, and $A \propto d^2$, so $\sigma_{c,max}$ (Eq. 1) is more sensitive to changes in diameter. Origination of a secondary branch in element 7 means that the change in diameter there (from 29 cm to 21 cm) is markedly greater than in any other segment (Table 1) causing $\sigma_{c,max}$ to occur in element 7. Stresses in other branch elements are not negligible, however, with the smallest value of σ_c being approximately one-third that of $\sigma_{c,max}$. Therefore, defects in the branch could cause other elements to pose the greatest risk to the climber.

4. Conclusions

A method for assessing branch safety during ascending and during falls has been demonstrated. The method involves finite element modeling of the branch, determination of ascending and falling loads, and the computation of safety factors. The method has been illustrated for an example branch and a range of ascending techniques and proficiencies, and a range of fall characteristics, all with an unorthodox anchor point 11.5 m from the trunk. Safety factors during an ascent and fall were as small as 3 and 1.2, respectively. Both safety factors are considered small because of potentially large uncertainties in the climber-rope-branch system, particularly with respect to branch material properties and unobservable branch defects like decay or cracks. Even though the branch did not fail during the unorthodox ascent, the small safety factors may have compromised climber safety. The unorthodox ascent indicates that arborists may not fully appreciate the potential for failure of an anchor point. A better understanding of loads during an ascent or fall, as well as of basic mechanical concepts (e.g., leverage, momentum, acceleration, potential and kinetic energy, etc.) may improve recognition of possibly dangerous situations before a climber ascends, reducing risk.

References

Adams, M., 2007. Safe and efficient tree ascent: doubled rope techniques (DdRT)? Arborist News 16 (3), 50–54.

Anonymous, 2013. American National Standard for Arboricultural Operations: Safety Requirements. American National Standards Institute, NY, New York.

Bathe, K.J., 2006. Finite Element Procedures. Prentice Hall.

Brüchert, F., Speck, O., Spatz, H.-C., 2003. Oscillations of plants' stems and their damping: theory and experimentation. Philos. Trans R. Soc. Lond. B Biol. Sci. 358 (August), 1487–1492. http://dx.doi.org/10.1098/rstb.2003.1348.

Castillo, D.N., Menéndez, C.K.C., 2009. Work-related fatalities associated with tree care operations — United States: 1992–2007. Morbid. Mortal. Weekly Rep. 58 (15), 389–393.

Glass, S.V., Zelinka, S.L., 2010. Moisture relations and physical properties of wood. Wood Handbook: Wood as an Engineering Material. General Technical Report (GTR-190). Forest Products Laboratory, Madison, Wisconsin, pp. 4.1–4.19 (http://doi.org/ General Technical Report FPL-GTR-190).

Kane, B., Clouston, P., 2008. Tree pulling tests of large shade trees in the genus Acer. Arboricult. Urban For. 34 (2), 101–109.

Kane, B., Ryan, H.D.P., 2004. The accuracy of formulas used to assess strength loss due to decay in trees. J. Arboric. 30 (6), 347–356.

Kane, B., 2007. Branch strength of Bradford pear (Pyrus calleryana var.'Bradford'). Arboricult. Urban For. 33 (4), 283–291.

Kane, B., 2014. Determining parameters related to the likelihood of failure of red oak (*Quercus rubra* L.) from winching tests. Trees − Struct. Funct. 28 (6), 1667–1677. http://dx.doi.org/10.1007/s00468-014-1076-0.

Kretschmann, D.E., 2010. Mechanical properties of wood. Wood Handbook – Wood as an Engineering Material. pp. 5.1–5.46. (Retrieved from). http://www.fpl.fs.fed.us/documnts/fplgtr/fplgtr190/chapter_05.pdf?.

Lilly, S., 2005. Tree Climber's Guide, 3rd ed. International Society of Arboriculture, Champaign, IL.

Niklas, K.J., 1997. Size- and age-dependent variation in the properties of sap- and heartwood in black locust (Robinia pseudoacacia L.). Ann. Bot. 79 (5), 473–478.

Okai, R., Frimpong-Mensah, K., Yeboah, D., 2004. Wood Sci. Technol. 38, 163. http://dx.doi.org/10.1007/s00226-004-0232-x.

Salmon, C.G., Johnson, J.E., 1990. Steel Structures: Design and Behavior, 3rd ed. Harper & Row, New York.

Wiatrowski, W.J., 2005. Fatalities in the Ornamental Shrub and Tree Services Industry. US Department of Labor, Bureau of Labor Statistics, Washington, DC (Available at). http://www.bls.gov/opub/mlr/cwc/fatalities-in-the-ornamental-shrub-and-tree-services-industry.pdf.